

Observation of $K^*(892)^0 \bar{K}^*(892)^0$ in χ_{cJ} Decays

M. Ablikim¹, J. Z. Bai¹, Y. Ban¹⁰, J. G. Bian¹, X. Cai¹, J. F. Chang¹, H. F. Chen¹⁶, H. S. Chen¹, H. X. Chen¹, J. C. Chen¹, Jin Chen¹, Jun Chen⁶, M. L. Chen¹, Y. B. Chen¹, S. P. Chi², Y. P. Chu¹, X. Z. Cui¹, H. L. Dai¹, Y. S. Dai¹⁸, Z. Y. Deng¹, L. Y. Dong¹, S. X. Du¹, Z. Z. Du¹, J. Fang¹, S. S. Fang², C. D. Fu¹, H. Y. Fu¹, C. S. Gao¹, Y. N. Gao¹⁴, M. Y. Gong¹, W. X. Gong¹, S. D. Gu¹, Y. N. Guo¹, Y. Q. Guo¹, Z. J. Guo¹⁵, F. A. Harris¹⁵, K. L. He¹, M. He¹¹, X. He¹, Y. K. Heng¹, H. M. Hu¹, T. Hu¹, G. S. Huang^{1†}, L. Huang⁶, X. P. Huang¹, X. B. Ji¹, Q. Y. Jia¹⁰, C. H. Jiang¹, X. S. Jiang¹, D. P. Jin¹, S. Jin¹, Y. Jin¹, Y. F. Lai¹, F. Li¹, G. Li¹, H. H. Li¹, J. Li¹, J. C. Li¹, Q. J. Li¹, R. B. Li¹, R. Y. Li¹, S. M. Li¹, W. G. Li¹, X. L. Li⁷, X. Q. Li⁹, X. S. Li¹⁴, Y. F. Liang¹³, H. B. Liao⁵, C. X. Liu¹, F. Liu⁵, Fang Liu¹⁶, H. M. Liu¹, J. B. Liu¹, J. P. Liu¹⁷, R. G. Liu¹, Z. A. Liu¹, Z. X. Liu¹, F. Lu¹, G. R. Lu⁴, J. G. Lu¹, C. L. Luo⁸, X. L. Luo¹, F. C. Ma⁷, J. M. Ma¹, L. L. Ma¹¹, Q. M. Ma¹, X. Y. Ma¹, Z. P. Mao¹, X. H. Mo¹, J. Nie¹, Z. D. Nie¹, S. L. Olsen¹⁵, H. P. Peng¹⁶, N. D. Qi¹, C. D. Qian¹², H. Qin⁸, J. F. Qiu¹, Z. Y. Ren¹, G. Rong¹, L. Y. Shan¹, L. Shang¹, D. L. Shen¹, X. Y. Shen¹, H. Y. Sheng¹, F. Shi¹, X. Shi¹⁰, H. S. Sun¹, S. S. Sun¹⁶, Y. Z. Sun¹, Z. J. Sun¹, X. Tang¹, N. Tao¹⁶, Y. R. Tian¹⁴, G. L. Tong¹, G. S. Varner¹⁵, D. Y. Wang¹, J. Z. Wang¹, K. Wang¹⁶, L. Wang¹, L. S. Wang¹, M. Wang¹, P. Wang¹, P. L. Wang¹, S. Z. Wang¹, W. F. Wang¹, Y. F. Wang¹, Zhe Wang¹, Z. Wang¹, Zheng Wang¹, Z. Y. Wang¹, C. L. Wei¹, D. H. Wei³, N. Wu¹, Y. M. Wu¹, X. M. Xia¹, X. X. Xie¹, B. Xin⁷, G. F. Xu¹, H. Xu¹, Y. Xu¹, S. T. Xue¹, M. L. Yan¹⁶, F. Yang⁹, H. X. Yang¹, J. Yang¹⁶, S. D. Yang¹, Y. X. Yang³, M. Ye¹, M. H. Ye², Y. X. Ye¹⁶, L. H. Yi⁶, Z. Y. Yi¹, C. S. Yu¹, G. W. Yu¹, C. Z. Yuan¹, J. M. Yuan¹, Y. Yuan¹, Q. Yue¹, S. L. Zang¹, Yu. Zeng¹, Y. Zeng⁶, B. X. Zhang¹, B. Y. Zhang¹, C. C. Zhang¹, D. H. Zhang¹, H. Y. Zhang¹, J. Zhang¹, J. Y. Zhang¹, J. W. Zhang¹, L. S. Zhang¹, Q. J. Zhang¹, S. Q. Zhang¹, X. M. Zhang¹, X. Y. Zhang¹¹, Y. J. Zhang¹⁰, Y. Y. Zhang¹, Yiyun Zhang¹³, Z. P. Zhang¹⁶, Z. Q. Zhang⁴, D. X. Zhao¹, J. B. Zhao¹, J. W. Zhao¹, M. G. Zhao⁹, P. P. Zhao¹, W. R. Zhao¹, X. J. Zhao¹, Y. B. Zhao¹, Z. G. Zhao^{1*}, H. Q. Zheng¹⁰, J. P. Zheng¹, L. S. Zheng¹, Z. P. Zheng¹, X. C. Zhong¹, B. Q. Zhou¹, G. M. Zhou¹, L. Zhou¹, N. F. Zhou¹, K. J. Zhu¹, Q. M. Zhu¹, Y. C. Zhu¹, Y. S. Zhu¹, Yingchun Zhu¹, Z. A. Zhu¹, B. A. Zhuang¹, B. S. Zou¹.

(BES Collaboration)

¹ *Institute of High Energy Physics, Beijing 100039, People's Republic of China*

² *China Center of Advanced Science and Technology, Beijing 100080, People's Republic of China*

³ *Guangxi Normal University, Guilin 541004, People's Republic of China*

⁴ *Henan Normal University, Xinxiang 453002, People's Republic of China*

⁵ *Huazhong Normal University, Wuhan 430079, People's Republic of China*

⁶ *Hunan University, Changsha 410082, People's Republic of China*

⁷ *Liaoning University, Shenyang 110036, People's Republic of China*

⁸ *Nanjing Normal University, Nanjing 210097, People's Republic of China*

⁹ *Nankai University, Tianjin 300071, People's Republic of China*

¹⁰ *Peking University, Beijing 100871, People's Republic of China*

¹¹ *Shandong University, Jinan 250100, People's Republic of China*

¹² *Shanghai Jiaotong University, Shanghai 200030, People's Republic of China*

¹³ *Sichuan University, Chengdu 610064, People's Republic of China*

¹⁴ *Tsinghua University, Beijing 100084, People's Republic of China*

¹⁵ *University of Hawaii, Honolulu, Hawaii 96822, USA*

¹⁶ *University of Science and Technology of China, Hefei 230026, People's Republic of China*

¹⁷ *Wuhan University, Wuhan 430072, People's Republic of China*

¹⁸ *Zhejiang University, Hangzhou 310028, People's Republic of China*

* *Visiting professor to University of Michigan, Ann Arbor, MI 48109, USA*

† *Current address: Purdue University, West Lafayette, Indiana 47907, USA.*

(Dated: November 16, 2018)

$K^*(892)^0 \bar{K}^*(892)^0$ signals from χ_{cJ} ($J = 0, 1, 2$) decays are observed for the first time using a data sample of 14 million $\psi(2S)$ events accumulated at the BESII detector. The branching fractions $\mathcal{B}(\chi_{cJ} \rightarrow K^*(892)^0 \bar{K}^*(892)^0)$ ($J = 0, 1, 2$) are determined to be $(1.55 \pm 0.35 \pm 0.30) \times 10^{-3}$, $(1.58 \pm 0.32 \pm 0.29) \times 10^{-3}$, and $(4.67 \pm 0.55 \pm 0.85) \times 10^{-3}$ for the χ_{c0} , χ_{c1} and χ_{c2} decays, respectively, where the first errors are statistical and the second are systematic. The significances of these signals are about 4.2σ , 4.3σ , and 7.5σ , respectively.

PACS numbers: 13.25.Gv, 12.38.Qk, 14.40.Gx

I. INTRODUCTION

Exclusive quarkonium decays constitute an interesting laboratory for investigating perturbative quantum chromodynamics (QCD). In the case of P -wave charmonium χ_{cJ} decays to a pair of pseudoscalars, one finds that the lowest Fock state, the color-singlet contribution, alone is not sufficient to accommodate the data. Indeed, it turns out that the color-octet contribution from the next higher Fock state contributes at the same level as the color singlet one. Its inclusion yields good agreement with experimental data [1,2]. The calculation of the partial width of $\chi_{cJ} \rightarrow p\bar{p}$, taking into account the color octet mechanism [3], also obtains results in reasonable agreement with measurements [4]. Nevertheless a recent measurement of the $\chi_{cJ} \rightarrow \Lambda\bar{\Lambda}$ [5] only agrees marginally with this prediction.

At present there are no predictions for the majority of the hadronic decay modes. In addition, few two-body decays have been measured. A consistent set of predictions for the branching fractions, as well as more precise experimental measurements, for a number of the two-body decays may lead to further insight into the nature of these 3P_J $c\bar{c}$ bound states.

In this paper, we report on the analysis of $\pi^+\pi^-K^+K^-$ final states from χ_{cJ} ($J = 0, 1, 2$) decays using 14 million $\psi(2S)$ events accumulated at the upgraded BES detector (BES II). Signals of χ_{c0} , χ_{c1} and χ_{c2} decays to $K^*(892)^0\bar{K}^*(892)^0$ in $\psi(2S)$ radiative decays are observed for the first time.

II. BES DETECTOR

BES II is a large solid-angle magnetic spectrometer that is described in detail in Ref. [6]. Charged particle momenta are determined with a resolution of $\sigma_p/p = 1.78\%\sqrt{1+p^2}$ (p in GeV/ c) in a 40-layer cylindrical drift chamber. Particle identification is accomplished by specific ionization (dE/dx) measurements in the drift chamber and time-of-flight (TOF) measurements in a barrel-like array of 48 scintillation counters. The dE/dx resolution is $\sigma_{dE/dx} = 8.0\%$; the TOF resolution is $\sigma_{TOF} = 180$ ps for Bhabha events. Outside of the time-of-flight counters is a 12-radiation-length barrel shower counter (BSC) comprised of gas proportional tubes interleaved with lead sheets. The BSC measures the energies of photons with a resolution of $\sigma_E/E \simeq 21\%/\sqrt{E}$ (E in GeV). Outside the solenoidal coil, which provides a 0.4 T magnetic field over the tracking volume, is an iron flux return that is instrumented with three double layers of counters that are used to identify muons.

In this analysis, a GEANT3 based Monte Carlo simulation package (SIMBES) with detailed consideration of detector performance (such as dead electronic channels) is used. The consistency between data and Monte Carlo has been checked in many high purity physics channels, and the agreement is quite reasonable.

III. EVENT SELECTION

The selection criteria described below are similar to those used in a previous BES analysis [7].

A. Photon identification

A neutral cluster is considered to be a photon candidate when the angle between the nearest charged track and the cluster is greater than 15° , the first hit is in the beginning six radiation lengths, and the difference between the angle of the cluster development direction in the BSC and the photon emission direction is less than 30° . The photon candidate with the largest energy deposit in the BSC is treated as the photon radiated from $\psi(2S)$ and used in a four-constraint kinematic fit to the hypothesis $\psi(2S) \rightarrow \gamma\pi^+\pi^-K^+K^-$.

B. Charged particle identification

Each charged track, reconstructed using the MDC information, is required to be well fit to a three-dimensional helix, be in the polar angle region $|\cos\theta_{MDC}| < 0.80$, and have the point of closest approach of the track to the beam axis be within 2 cm of the beam axis and within 20 cm from the center of the interaction region along the beam line. For each track, the TOF and dE/dx measurements are used to calculate χ^2 values and the corresponding confidence levels for the hypotheses that the particle is a pion, kaon or proton (Prob_π , Prob_K , Prob_p).

C. Event selection criteria

Candidate events are required to satisfy the following selection criteria:

- (1) The number of charged tracks is required to be four with net charge zero.
- (2) The sum of the momenta of the two lowest momentum tracks is required to be greater than 650 MeV; this removes contamination from $\psi(2S) \rightarrow \pi^+\pi^- J/\psi$ events and some of the $\rho^0\pi\pi$ background.
- (3) The χ^2 probability for the four-constraint kinematic fit to the decay hypothesis $\psi(2S) \rightarrow \gamma\pi^+\pi^-K^+K^-$ is required to be greater than 0.01.

A combined probability determined from the four-constraint kinematic fit and particle identification information is used to separate $\gamma\pi^+\pi^-\pi^+\pi^-$, $\gamma K^+K^-K^+K^-$, and the different possible particle assignments for the $\gamma\pi^+\pi^-K^+K^-$ final states. This combined probability, Prob_{all} , is defined as

$$\text{Prob}_{all} = \text{Prob}(\chi_{all}^2, \text{ndf}_{all}),$$

where χ_{all}^2 is the sum of the χ^2 values from the four-constraint kinematic fit and those from each of the four particle identification assignments, and ndf_{all} is the corresponding total number of degrees of freedom. For an event to be selected, Prob_{all} of the $\gamma\pi^+\pi^-K^+K^-$ must be larger than those of the other possibilities. In addition, the particle identification probability of each charged track Prob_{ID} must be > 0.01 .

The invariant mass distribution for the $\pi^+\pi^-K^+K^-$ events that survive all the selection requirements is shown in Fig. 1. There are clear peaks corresponding to the χ_{cJ} states. The highest mass peak corresponds to charged tracks final states that are kinematically fit with an unassociated, low energy photon.

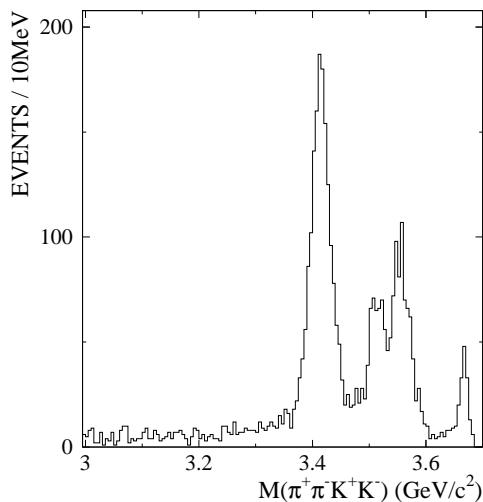


FIG. 1: The $\pi^+\pi^-K^+K^-$ invariant mass spectrum.

IV. ANALYSIS RESULTS

The scatter plots of $K^-\pi^+$ versus $K^+\pi^-$ invariant masses for events with a $\pi^+\pi^-K^+K^-$ mass within (3.30, 3.48) GeV, (3.48, 3.53) GeV and (3.53, 3.65) GeV are shown in Fig. 2. Clear $K^*(892)^0\bar{K}^*(892)^0$ signals can be seen in all χ_{cJ} decays, as well as some hints of $K_2^*(1430)K_2^*(1430)$ (or $K_0^*(1430)K_0^*(1430)$) and $K_1(1270)K$ (or $K_1(1400)K$) signals. In this paper, we study $K^*(892)^0\bar{K}^*(892)^0$ production in $\chi_{c0,1,2}$ decays.

A. $K^*(892)^0\bar{K}^*(892)^0$ signal

For the events in χ_{cJ} mass region (3.30, 3.65) GeV, after requiring that the mass of either (or both) $K\pi$ pair lies between 0.836 and 0.956 GeV, the mass distribution of the other $K\pi$ pair, shown in Fig. 3, is obtained; there is a strong $K^*(892)$ signal. The distribution is fitted with a background polynomial plus a P -wave relativistic Breit-Wigner

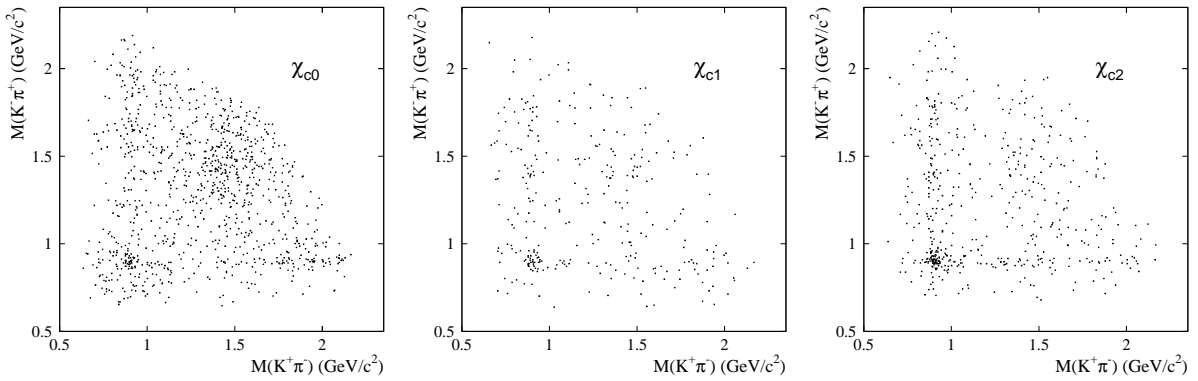


FIG. 2: Scatter plots of $K^-\pi^+$ versus $K^+\pi^-$ invariant masses for selected $\gamma\pi^+\pi^-K^+K^-$ events with $\pi^+\pi^-K^+K^-$ mass in χ_{c0} , χ_{c1} , and χ_{c2} mass regions, respectively.

function, with a width

$$\Gamma = \Gamma_0 \frac{m_0}{m} \frac{1 + r^2 p_0^2}{1 + r^2 p^2} \left[\frac{p}{p_0} \right]^3,$$

where m is the mass of the $K\pi$ system, p is the momentum of kaon in the $K\pi$ system, Γ_0 is the width of the resonance, m_0 is the mass of the resonance, p_0 is p evaluated at the resonance mass, r is the interaction radius, and $\frac{1 + r^2 p_0^2}{1 + r^2 p^2}$ represents the contribution of the barrier factor. The fit of Fig. 3 gives an r value of $(3.4 \pm 2.6) \text{ GeV}^{-1}$ with a large error due to the low statistics. Therefore, in later analysis (mainly in the efficiency calculation), we use the value $(3.4 \pm 0.6 \pm 0.3) \text{ GeV}^{-1}$ measured by the $K^-\pi^+$ scattering experiment [8] for r .

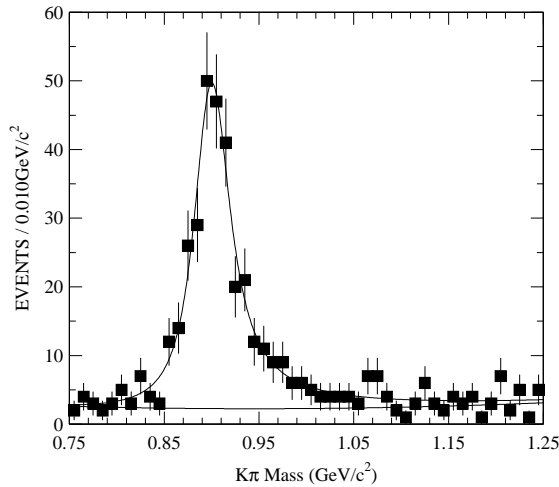


FIG. 3: $K\pi$ invariant mass spectrum recoiling against $K^*(892)$ ($0.836 \text{ GeV} < m_{K\pi} < 0.956 \text{ GeV}$) for events in the χ_{cJ} mass region (some events appear twice), where the curves are the Breit-Wigner function and background polynomial described in the text.

In this paper, the number of $K^*(892)^0 \bar{K}^*(892)^0$ events and the corresponding background are estimated from the scatter plot of $K^-\pi^+$ versus $K^+\pi^-$ invariant masses, as shown in Fig. 4. The signal region is shown as a square box (solid line) at $(0.896, 0.896) \text{ GeV}$ with the width of 60 MeV. From a Monte Carlo study, a large background comes from $\psi(2S) \rightarrow \gamma\chi_{cJ} \rightarrow \gamma K_1(1270)K$ (or $K_1(1400)K$) which decays to $\gamma\pi^+\pi^-K^+K^-$ final states via $K_1 \rightarrow K^*(892)\pi$ intermediate decay. This background shows up as the horizontal and vertical bands at $m(K^*(892))$ in the $m(K^-\pi^+)$ versus $m(K^+\pi^-)$ scatter plots of Fig. 2. Hence, backgrounds are estimated from sideband boxes, which are taken 60 MeV away from the signal box and shown as four dashed-line boxes in Fig. 4. Background in the horizontal or vertical sideband boxes is twice that in the signal region.

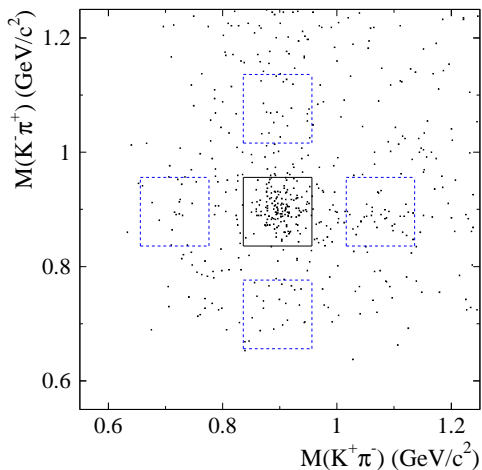


FIG. 4: Definition of signal and sideband regions.

Figure 5 shows the mass distribution of the $K^*(892)^0 \bar{K}^*(892)^0$ candidate events and the corresponding background. There are 154 and 46 (92/2) events obtained from the signal box and the dashed-line boxes within 3.20 GeV - 3.70 GeV, respectively.

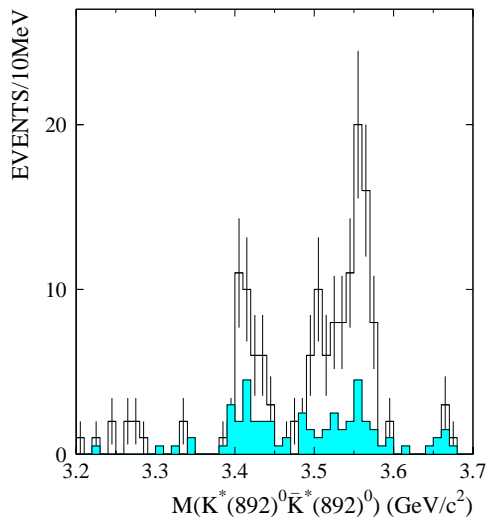


FIG. 5: The $K^*(892)^0 \bar{K}^*(892)^0$ invariant mass spectrum for events in the signal region of Fig. 4. The shaded histogram indicates the distribution of the background estimated for events in the sideband regions of Fig. 4.

B. Fit of the mass spectrum

After sideband subtraction, the $K^*(892)^0 \bar{K}^*(892)^0$ mass spectrum between 3.20 and 3.70 GeV is fitted using a χ^2 method with three Breit-Wigner functions folded with Gaussian resolutions, where the mass resolutions are fixed at their Monte Carlo predicted values [(12.2 \pm 0.4) MeV, (12.3 \pm 0.3) MeV and (12.2 \pm 0.3) MeV for χ_{c0} , χ_{c1} and χ_{c2} , respectively] and the widths of the three χ_{cJ} states are set at their world average values [4]. A χ^2 probability of 70% is obtained, indicating a reliable fit. The number of events determined from the fit are 26.1 ± 5.8 , 26.9 ± 5.4 and 55.1 ± 6.3 for χ_{c0} , χ_{c1} , and χ_{c2} , respectively. The statistical significances of the three states are 4.2σ , 4.3σ and 7.5σ , calculated from $\sqrt{\Delta\chi^2}$, where $\Delta\chi^2$ is the difference between the χ^2 values of the fits determined with and without the signal function. Fig. 6 shows the fit result, and the fitted masses are 3416.2 ± 3.6 MeV, 3507.8 ± 3.6 MeV and 3553.6 ± 1.8 MeV for χ_{c0} , χ_{c1} and χ_{c2} , respectively, in agreement with the world average values [4].

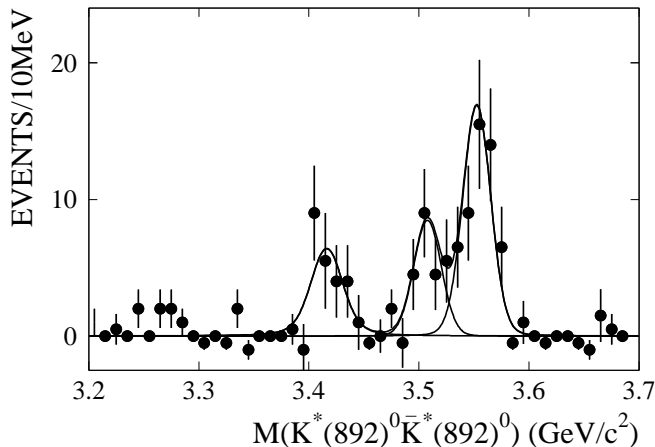


FIG. 6: The $K^*(892)^0 \bar{K}^*(892)^0$ invariant mass spectrum fitted with three resolution smeared Breit-Wigner functions as described in the text.

A Monte Carlo simulation is used to determine the detection efficiency. The angular distribution of the photon emitted in $\psi(2S) \rightarrow \gamma \chi_{c0}$ is taken into account [9]. The $K^*(892)$ is generated as a P -wave relativistic Breit-Wigner with r as 3.4 GeV^{-1} [8]. For each case, 50,000 Monte Carlo events are simulated, and the efficiencies are estimated to be $\epsilon_{\chi_{c0}} = (3.15 \pm 0.09)\%$, $\epsilon_{\chi_{c1}} = (3.25 \pm 0.09)\%$, and $\epsilon_{\chi_{c2}} = (2.96 \pm 0.08)\%$, where the error is the statistical error of the Monte Carlo sample. Note that for the efficiency estimation, the events in the four sideband boxes are subtracted from the events in the signal region of the scatter plot, similar to the treatment of data.

The branching fraction of $\psi(2S) \rightarrow \gamma \chi_{cJ}$, $\chi_{cJ} \rightarrow K^*(892)^0 \bar{K}^*(892)^0$ is calculated using

$$\mathcal{B}(\chi_{cJ} \rightarrow \gamma \chi_{cJ} \rightarrow \gamma K^*(892)^0 \bar{K}^*(892)^0) = \frac{n^{obs}/(\epsilon \cdot f^2)}{N_{\psi(2S)}},$$

where the factor f is the branching fraction of $K^*(892)^0$ to the charged $K\pi$ mode, which is taken as $\frac{2}{3}$.

Using the numbers obtained above and the total number of $\psi(2S)$ events, $14.0 (1.00 \pm 0.04) \times 10^6$ [10], we determine the following branching fractions

$$\mathcal{B}(\psi(2S) \rightarrow \gamma \chi_{c0} \rightarrow \gamma K^*(892)^0 \bar{K}^*(892)^0) = (1.33 \pm 0.30) \times 10^{-4},$$

$$\mathcal{B}(\psi(2S) \rightarrow \gamma \chi_{c1} \rightarrow \gamma K^*(892)^0 \bar{K}^*(892)^0) = (1.33 \pm 0.27) \times 10^{-4},$$

$$\mathcal{B}(\psi(2S) \rightarrow \gamma \chi_{c2} \rightarrow \gamma K^*(892)^0 \bar{K}^*(892)^0) = (2.99 \pm 0.35) \times 10^{-4},$$

where the errors are statistical only.

C. Systematic errors

The systematic errors in the branching fraction measurement associated with the efficiency are determined by comparing $\psi(2S)$ data and Monte Carlo simulation for very clean decay channels, such as $\psi(2S) \rightarrow \pi^+ \pi^- J/\psi$, which allows the determination of systematic errors associated with the MDC tracking, kinematic fitting, particle identification, and efficiency of the photon ID [11]. Other sources of systematic error come from the uncertainties in the number of $\psi(2S)$ events [10], the efficiency estimation using simulated data, the background, the χ_{cJ} and $K^*(892)^0$ mass resolutions, the binning and fit range, etc.

1. Efficiency estimation

As mentioned above, we use the measurement of Ref. [8], $(3.4 \pm 0.6 \pm 0.3) \text{ GeV}^{-1}$ for r in the P -wave relativistic Breit-Wigner parameterization in the Monte Carlo simulation. We also use r varied by one sigma to 2.73 GeV^{-1} and

4.07 GeV⁻¹ to determine the change in the detection efficiency. For $r = 2.73$ GeV⁻¹, the efficiencies of the χ_{c0} , χ_{c1} , and χ_{c2} become 2.90%, 2.99% and 2.74%, and for $r = 4.07$ GeV⁻¹, the corresponding efficiencies are 3.37%, 3.52%, and 3.16%, respectively. The largest changes are about 7.9%, 8.3% and 7.4% for χ_{c0} , χ_{c1} and χ_{c2} .

2. Background subtraction

In Section IV A, the backgrounds are estimated using the sidebands shown as the four dashed-line boxes in Fig. 4. Moving the sideband boxes 20 MeV away from or closer to the signal region, or varying the background number by one standard deviation, the largest changes of the branching fractions for the χ_{c0} , χ_{c1} and χ_{c2} are about 7.4%, 5.0% and 5.5%, respectively, obtained by re-fitting the $K^*(892)^0 \bar{K}^*(892)^0$ mass spectrum and reestimating the efficiency.

3. χ_{cJ} and $K^*(892)^0$ mass resolutions

Differences between data and Monte Carlo for the mass resolutions of the χ_{cJ} or $K^*(892)^0$ also give uncertainties in the determination of the branching fractions. The maximum possible difference for χ_{cJ} is about 1 MeV. Such a change results in about 4.5%, 2.5% and 2.0% variations in the fitted number of χ_{c0} , χ_{c1} , and χ_{c2} events. If we change the $K^*(892)^0$ window to $[0.836 + 0.002, 0.956 - 0.002]$ GeV and $[0.836 - 0.002, 0.956 + 0.002]$ GeV, the efficiency variations of the χ_{c0} , χ_{c1} and χ_{c2} are 1.5%, 2.5% and 2.4%, respectively. By varying the width of χ_{c0} by 1σ , 0.8 MeV, there is almost no change in the final fit result. We use total systematic errors of 5%, 3.5% and 3.5% for this uncertainty.

4. Binning and fit range

Using different binning and fit ranges for the $K^*(892)^0 \bar{K}^*(892)^0$ mass spectrum fit yields errors of about 4%, 2% and 2% for χ_{c0} , χ_{c1} and χ_{c2} , respectively.

TABLE I: Summary of systematic errors in the branching fraction calculation of $\mathcal{B}(\psi(2S) \rightarrow \gamma\chi_{cJ} \rightarrow \gamma K^*(892)^0 \bar{K}^*(892)^0)$.

Source	χ_{c0}	χ_{c1}	χ_{c2}
MDC tracking	8%	8%	8%
Kinematic fit	6%	6%	6%
Particle identification	5%	5%	5%
Photon ID efficiency	2%	2%	2%
$\psi(2S)$ number	4%	4%	4%
Efficiency estimation	7.9%	8.3%	7.4%
Background	7.3%	5.0%	5.5%
Mass resolutions	5%	3.5%	3.5%
Binning and fit range	4%	2%	2%
Total systematic error	17.4%	16.0%	15.7%

The systematic errors from all sources are listed in Table I, as are the total errors of 17.4%, 16.0% and 15.7% for χ_{c0} , χ_{c1} and χ_{c2} , respectively, obtained by adding them in quadrature. The resulting branching fractions are

$$\mathcal{B}(\psi(2S) \rightarrow \gamma\chi_{c0} \rightarrow \gamma K^*(892)^0 \bar{K}^*(892)^0) = (1.33 \pm 0.30 \pm 0.23) \times 10^{-4},$$

$$\mathcal{B}(\psi(2S) \rightarrow \gamma\chi_{c1} \rightarrow \gamma K^*(892)^0 \bar{K}^*(892)^0) = (1.33 \pm 0.27 \pm 0.21) \times 10^{-4},$$

$$\mathcal{B}(\psi(2S) \rightarrow \gamma\chi_{c2} \rightarrow \gamma K^*(892)^0 \bar{K}^*(892)^0) = (2.99 \pm 0.35 \pm 0.47) \times 10^{-4},$$

and with the PDG world average values of $\psi(2S) \rightarrow \gamma\chi_{cJ}$ [4], we get the following branching fractions

$$\mathcal{B}(\chi_{c0} \rightarrow K^*(892)^0 \bar{K}^*(892)^0) = (1.55 \pm 0.35 \pm 0.30) \times 10^{-3},$$

TABLE II: Summary of numbers used in the branching fraction calculation and branching fraction results.

Quantity	χ_{c0}	χ_{c1}	χ_{c2}
n^{obs}	26.1 ± 5.8	26.9 ± 5.4	55.1 ± 6.3
ϵ (%)	3.15 ± 0.09	3.25 ± 0.09	2.96 ± 0.08
$N_{\psi(2S)}$ (10^6) [10]	14.0 ± 0.6	14.0 ± 0.6	14.0 ± 0.6
f	$\frac{2}{3}$	$\frac{2}{3}$	$\frac{2}{3}$
$\mathcal{B}(\psi(2S) \rightarrow \gamma\chi_{cJ})$ (%) [4]	8.6 ± 0.7	8.4 ± 0.8	6.4 ± 0.6
$\mathcal{B}(\chi_{cJ} \rightarrow K^*(892)^0 \bar{K}^*(892)^0)$ (10^{-3})	$1.55 \pm 0.35 \pm 0.30$	$1.58 \pm 0.32 \pm 0.29$	$4.67 \pm 0.55 \pm 0.85$

$$\mathcal{B}(\chi_{c1} \rightarrow K^*(892)^0 \bar{K}^*(892)^0) = (1.58 \pm 0.32 \pm 0.29) \times 10^{-3},$$

$$\mathcal{B}(\chi_{c2} \rightarrow K^*(892)^0 \bar{K}^*(892)^0) = (4.67 \pm 0.55 \pm 0.85) \times 10^{-3},$$

where the first error is statistical and the second is systematic. The numbers used and results are summarized in Table II.

V. SUMMARY

In summary, $K^*(892)^0 \bar{K}^*(892)^0$ signals from χ_{cJ} ($J = 0, 1, 2$) decays are observed for the first time using a sample of 14 million $\psi(2S)$ events accumulated at the BESII detector. The branching fractions are determined to be $\mathcal{B}(\chi_{c0} \rightarrow K^*(892)^0 \bar{K}^*(892)^0) = (1.55 \pm 0.35 \text{ (stat)} \pm 0.30 \text{ (syst)}) \times 10^{-3}$, $\mathcal{B}(\chi_{c1} \rightarrow K^*(892)^0 \bar{K}^*(892)^0) = (1.58 \pm 0.32 \text{ (stat)} \pm 0.29 \text{ (syst)}) \times 10^{-3}$, and $\mathcal{B}(\chi_{c2} \rightarrow K^*(892)^0 \bar{K}^*(892)^0) = (4.67 \pm 0.55 \text{ (stat)} \pm 0.85 \text{ (syst)}) \times 10^{-3}$; and the significances of the $K^*(892)^0 \bar{K}^*(892)^0$ signals are about 4.2σ , 4.3σ and 7.5σ for the $\chi_{c0,1,2}$ decays, respectively. This will be helpful in understanding the nature of χ_c states.

VI. ACKNOWLEDGEMENTS

The BES collaboration thanks the staff of BEPC for their hard efforts. This work is supported in part by the National Natural Science Foundation of China under contracts Nos. 19991480, 10225524, 10225525, the Chinese Academy of Sciences under contract No. KJ 95T-03, the 100 Talents Program of CAS under Contract Nos. U-11, U-24, U-25, and the Knowledge Innovation Project of CAS under Contract Nos. U-602, U-34 (IHEP); by the National Natural Science Foundation of China under Contract No. 10175060 (USTC), and No. 10225522 (Tsinghua University); and by the Department of Energy under Contract No. DE-FG03-94ER40833 (U Hawaii).

-
- [1] G.T. Bodwin, E. Braaten and G.P. Lepage, Phys. Rev. D **51** (1995) 1125; J. Bolz, P. Koll and G.A. Schuler, Phys. Lett. B **392** (1997) 198; G.A. Schuler, Nucl. Phys. Proc. Suppl. **64** (1998) 450.
 - [2] J.Z. Bai *et al.* (BES Collaboration), Phys. Rev. Lett. **81** (1998) 3091.
 - [3] S.M.H. Wong, Eur. Phys. J. C **14** (2000) 643.
 - [4] S. Eidelman *et al.* (Particle Data Group), Phys. Lett. B **592** (2004) 1.
 - [5] J.Z. Bai *et al.* (BES Collaboration), Phys. Rev. D **67** (2003) 112001.
 - [6] J.Z. Bai *et al.* (BES Collaboration), Nucl. Instrum. Meth. A **458** (2001) 627.
 - [7] J.Z. Bai *et al.* (BES Collaboration), Phys. Rev. D **60** (1999) 072001.
 - [8] D. Aston *et al.*, Nucl. Phys. B **296** (1988) 493.
 - [9] W. Tanenbaum *et al.* (Mark I Collaboration), Phys. Rev. D **17** (1978) 1731; G. Karl, S. Meshkov and J.L. Rosner, *ibid.* D **13** (1976) 1203; M. Oreglia *et al.* (Crystal Ball Collaboration), *ibid.* D **25** (1982) 2259.
 - [10] X.H. Mo *et al.*, High Energy Phys. Nucl. Phys. **28** (2004) 455.
 - [11] J.Z. Bai *et al.* (BES Collaboration), Phys. Rev. D **69** (2004) 012003.